Ultra-sensitive NEMS-based cantilevers for sensing, scanned probe and very high-frequency applications

MO LI, H. X. TANG* AND M. L. ROUKES†

Kavli Nanoscience Institute and Departments of Physics, Applied Physics, and Bioengineering, California Institute of Technology, MS 114-36, Pasadena, California 91125, USA

*Present address: Departments of Electrical Engineering and Mechanical Engineering, Yale University, Becton Center 215, 15 Prospect St, New Haven, Connecticut 06520, USA

†e-mail: roukes@caltech.edu

Published online: 28 January 2007; doi:10.1038/nnano.2006.208

Scanning probe microscopies (SPM) and cantilever-based sensors generally use low-frequency mechanical devices of microscale dimensions or larger. Almost universally, off-chip methods are used to sense displacement in these devices, but this approach is not suitable for nanoscale devices. Nanoscale mechanical sensors offer a greatly enhanced performance that is unattainable with microscale devices. Here we describe the fabrication and operation of self-sensing nanocantilevers with fundamental mechanical resonances up to very high frequencies (VHF). These devices use integrated electronic displacement transducers based on piezoresistive thin metal films, permitting straightforward and optimal nanodevice readout. This non-optical transduction enables applications requiring previously inaccessible sensitivity and bandwidth, such as fast SPM and VHF force sensing. Detection of 127 MHz cantilever vibrations is demonstrated with a thermomechanical-noise-limited displacement sensitivity of 39 fm $Hz^{-1/2}$. Our smallest devices, with dimensions approaching the mean free path at atmospheric pressure, maintain high resonance quality factors in ambient conditions. This enables chemisorption measurements in air at room temperature, with unprecedented mass resolution less than 1 attogram (10^{-18} g).

In the mid-1980s, microcantilever force sensors enabled the development of atomic force microscopy (AFM)[1]. Within a very short period of time, atomic resolution was attained[2], and the atomic force microscope is now one of the most important tools in nanoscience[3,4]. Perhaps equally important is that the advent of AFM has led to the growth of the wider field of cantilever-based sensing, including a wide range of scanning probe microscopies (SPM), and many different forms of static (that is, non-scanned) sensing. Today's SPM can be used to image local forces arising from magnetic and magnetic resonance interactions; forces from local electrostatics, surface potentials, surface temperatures, and chemical bonding; and forces from many other local origins. Similarly, applications for non-scanned microcantilever sensors are equally diverse, including infrared imaging, nanocalorimetry, vapour- and liquid-phase chemisensing, electrometry, mass detection and many others[5–7].

At microscale dimensions the practical upper limit to fundamental-mode cantilever resonant frequencies is generally of the order of several megahertz[8]. For SPM this imposes a substantial limitation upon scan rate, which directly determines the speed at which images can be acquired. Moreover, the standard approaches used to make microelectromechanical systems (MEMS) cannot provide access to the nanoscale, where very large improvements in sensitivity can be attained[9]. Recent demonstrations and applications of the unprecedented sensitivity available from nanoelectromechanical (NEMS) devices include milestones such as sub-single-charge electrometry[10], single-electron-spin paramagnetic resonance[11], zeptogram-scale mass sensing[12], zeptonewton-scale force sensing[13] and subfemtometre displacement sensing[14]. In fact, with these continuing advances, NEMS sensors are rapidly converging towards the ultimate, quantum limits of force and displacement detection[15].

However, in contrast to MEMS, NEMS devices are still largely pursued only within the province of specialists. A current barrier to their practical development and widespread use is the difficulty of achieving sensitive displacement transduction at the nanoscale. Beyond the initial challenges of fabricating ultrasmall mechanical devices, successful realization of NEMS involves addressing the doubly hard challenge of realizing very high frequency displacement sensing while attaining extreme subnanometre resolution. This is not straightforward; approaches to displacement transduction commonly used for MEMS generally are not applicable to NEMS[9]. For example, the efficiency of capacitive detection precipitously decreases at the nanoscale, and the signal is typically overwhelmed by uncontrollable parasitic effects. For optical readouts, diffraction effects become pronounced when device dimensions are scaled far below the wavelength of the illumination used. Furthermore, existing readouts for scanned probe microscopy cantilevers are predominantly based upon external (that is, off-chip) displacement sensing systems that, typically, greatly exceed the size scale of the cantilever sensors themselves. The most common SPM readouts are optically based, involving simple optical

©2007 Nature Publishing Group

beam deflection or more sensitive interferometry. By comparison, only a relatively small subset of efforts has focused upon development of self-sensing nanocantilevers. The optimization of integrated displacement transduction for nanoscale mechanical devices is central to this work.

DISPLACEMENT TRANSDUCTION FOR NANODEVICES

To date, most self-sensing microcantilevers use piezoresistive displacement transduction[16]. A sensor patterned from piezoresistive material, affixed to moving parts of a mechanical device, undergoes a resistance change in response to the motion-induced strain. Current biasing such a piezoresistor translates the strain-induced resistance change into a measurable voltage. The integration of such displacement sensors with the mechanical elements eliminates the need for device alignment with an (otherwise) external readout, such as a laser. This brings immense simplification to instrument design. Even more important, however, is that, by circumventing optics, piezoresistive transduction yields access to dimensions far below the diffraction limit, where the substantial advantages of nanoscale sensors are available. However several important issues must be addressed to make this possible.

Previous efforts to optimize piezoresistive sensors have largely focused upon use of doped semiconducting materials, as they can provide a very large gauge factor, $\gamma = (\mathrm{d}R/R)/\varepsilon$, which is the figure of merit for piezoresistive material. Here R and ε are the resistance of and the strain in the piezoresistive sensor, respectively. The parameter γ quantifies the (normalized) resistance change that arises in response to applied strain; nominally, a larger γ yields better 'strain-to-resistance conversion' from the transducer. It is widely assumed that optimal transducer performance is obtained simply by using materials offering maximal γ. This assumption is profoundly incorrect for nanoscale sensors.

Two distinct mechanisms generate piezoresistivity in a conducting material. First, reversible elastic deformation of the material results in a change to the conduction geometry and this, in turn, always gives rise to a modest change in resistance. Second, perturbation of the intrinsic conduction mechanisms arises from dilatation of a material; this change, by comparison, can be very large in certain cases. These separate and distinct effects, respectively, are represented by the first and second terms on the right side of the expression[17]

$$\gamma = \frac{\mathrm{d}R}{R}\frac{1}{\varepsilon} = (1+\nu) + \frac{\partial\rho}{\rho}\frac{1}{\varepsilon} \qquad (1)$$

Here ν is the material's Poisson's ratio and ρ is its resistivity. The first term on the right in equation (1) is typically only of order 1 or 2 for typical thin-film conductors; however, whereas the second term is also of order unity in metals, it can range from tens to several thousand in semiconductors depending upon the doping level and conduction mechanism[18]. This term is reportedly increased in extremely thin films (<2 nm) (ref. 19), and close to the metal–insulator transition, γ actually diverges[20].

The commonly held assumption is that a large gauge factor will serve to maximize a displacement sensor's performance, but this is actually only one element in optimizing its transduction efficiency. There are three generic attributes of high-γ materials that are always deleterious to high-sensitivity displacement transduction. The first is that high γ is generally achieved only with high-resistivity materials and, hence, large, two-terminal resistances are quickly attained when the size of a piezoresistive transducer patterned from such materials is scaled down to nanometre dimensions. This can make noise matching between nanoscale piezoresistors and readout circuitry extremely difficult, or impossible, especially at high frequencies. In fact, below a particular size range set by the carrier depletion length, surface states in semiconducting transducers can render them susceptible to freeze-out at reduced temperatures, or, in the worst case, non-conducting even at room temperature. A second issue, in fact related to the first, is that high γ is typically associated with very low carrier densities and, hence, often with highly disordered or percolative conduction. When such a piezoresistor is scaled downward in size, its resistance increase is accompanied by a very large increase in low frequency 'flicker' noise, as described by Hooge's relation[21], $S_R^{(1/f)} = 2\pi\zeta R^2/(N\omega)$. This empirical relation describes how the spectral density of resistance fluctuations at angular frequency ω grows when the number of carriers becomes small. Here N is the number of carriers within the sample of resistance R, and ζ is a sample-specific materials parameter (for p^+ Si, $\zeta \sim 10^{-5}$) (ref. 22). Finally, a third deleterious attribute of high-γ materials is their large temperature coefficients. These, too, originate from the low carrier density in the semiconducting (compared with metallic) regime, and the thermally activated, defect-mediated transport that is involved.

MATCHING TO NANOSCALE TRANSDUCERS

These issues become very problematic for nanoscale piezoresistors. We find they may be circumvented, thereby enabling the immense advantages of self-sensing detection in the nanoscale regime, by replacing the conventionally used semiconducting piezoresistive layer with a thin metal film. The underlying rationale for this replacement elucidates the true figure of merit for piezoresistive displacement transduction. It is not gauge factor, but output (voltage domain) signal-to-noise ratio (SNR), which also takes into account the coupling efficiency attained between the displacement transducer and its subsequent readout. Specifically, for a nanoscale device, the loss of a factor of $\sim$20 in γ that results when changing from a semiconducting to a metallic transducer is amply compensated by a profound reduction in the resistance of the latter, which can be a factor of $\sim 10^4$ or more. The latter arises directly from the huge disparity between the carrier density in thin metal films compared with that of doped semiconductor layers.

Use of metallic-density elements immensely simplifies impedance matching between the transducer and its subsequent readout, whose quality we characterize by the transmission coefficient, $1-\Gamma(Z_L, Z_0)$ at their juncture. Here, $\Gamma = (Z_L - Z_0)/(Z_L + Z_0)$ is the junction reflection coefficient and Z_L and Z_0 are the impedances of the transducer output and the readout input. Typically, Z_0 is 50 Ω for a low-noise, high-frequency amplifier. Invariably, for high-impedance semiconducting devices of nanoscale dimensions, $Z_L \gg Z_0$; consequently $\Gamma \sim 1$ and most of the signal is lost by reflection at the readout's input. With nanoscale, metallic-density transducers we can engineer $Z_L \sim Z_0$, so that the transduced signal is optimally transmitted ($\Gamma \ll 1$). Further, low transducer output impedances provide greatly reduced susceptibility to signal degradation from inevitable parasitic reactances.

Additional collateral benefits of low-resistivity, metallic-density piezoresistors are their substantially reduced noise and their low drift. Further, these materials permit immense simplification of fabrication given their ease of deposition and patterning at the micro- and nanoscale. Their conductivity is robust against a wide range of chemical and plasma-based process conditions, in stark contrast to the well-known susceptibility of ultra-thin low-density semiconducting layers to such processes.

©2007 Nature Publishing Group

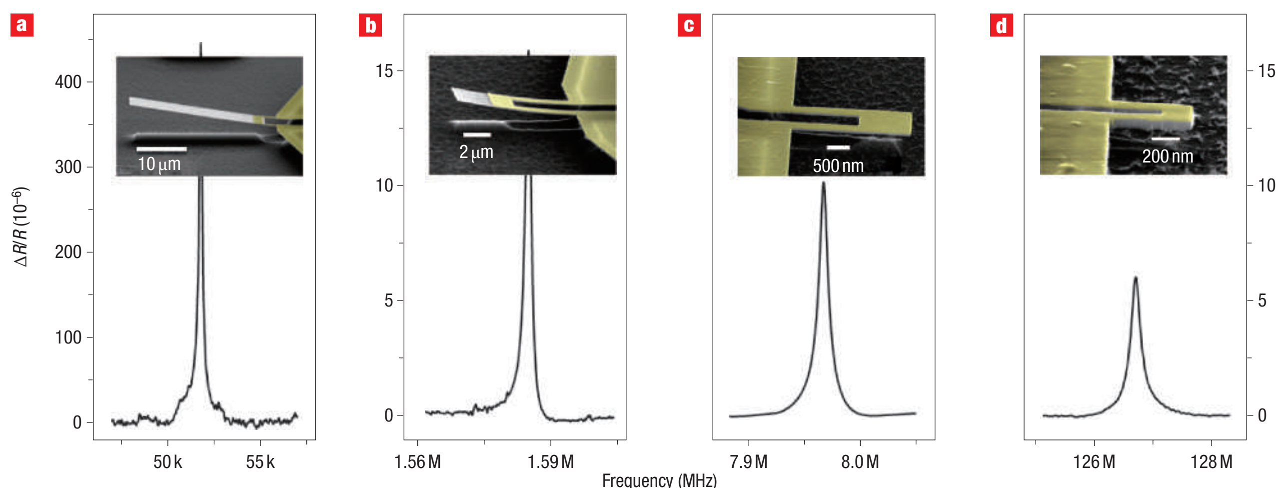

Figure 1 Piezoresistively detected resonant response from a family of SiC nanocantilevers to a 1 nN a.c. drive signal versus frequency, at room temperature in vacuum. Data are plotted as a normalized change in resistance; R is the d.c. transducer resistance. **a–d**, Fundamental-mode resonance frequencies are 52.1 kHz (**a**), 1.6 MHz (**b**), 8 MHz (**c**) and 127 MHz (**d**). The insets show SEM micrographs (angled perspective) of the devices, with dimensions 33 µm × 5 µm, 10 µm × 2 µm, 2.5 µm × 0.8 µm and 0.6 µm × 0.4 µm, respectively. All are fabricated from a single-crystal, 70-nm-thick SiC epilayer; the transducer metallization is colourized for clarity.

In the following we describe use of thin metal films to fabricate integrated transducers on the highest frequency nanoscale cantilevers reported to date—operating at up to the VHF band (~30–300 MHz)—and yielding performance at the thermodynamic limit of sensitivity. We anticipate that metallic-density transducers will find a wide variety of applications in sensing at the nanoscale, beyond those described here.

SELF-SENSING VHF NANOCANTILEVERS

Our self-sensing nanocantilevers are fabricated using a simple procedure that is readily amenable to mass fabrication and involves only two process steps. The insets of Fig. 1 are scanning electron microscope (SEM) images of four typical devices, with lengths varying from 600 nm to 30 µm and widths from 400 nm to 5 µm (Table 1). The cantilevers are supported by two narrow legs that serve both as an electrical path for piezoresistive transduction and, upon cantilever deflection, as strain concentrators[23]. In our cantilever design, which is based upon finite-element numerical methods[24], we simultaneously optimize for desired frequency, suppression of unwanted mechanical modes, and the maximization of deflection within the narrow transducers (legs) while minimizing their two-terminal resistance. By design, typical two-terminal resistances for completed devices are below 100 Ω. Frequency–response curves at fundamental resonance for the cantilever family of Fig. 1 are also displayed. It is evident that metallic piezoresistive detection is well suited to nanomechanical devices over a wide range of geometries and operating frequencies.

ULTRA-LOW TRANSDUCER NOISE

In contrast to nanocantilevers employing doped silicon piezoresistive transducers, electrical noise at low frequencies is extremely small in our devices. Low-frequency noise spectra from the two smallest self-sensing cantilevers (the devices of Fig. 1c, d) are displayed in Fig. 2a. To obtain these data, an a.c. bridge technique is used to extend the frequency range of noise-matched measurement down to ~1 MHz by heterodyning up in frequency, away from the readout amplifier's flicker noise regime[25]. Comparing published low-frequency noise data for typical doped silicon devices (upon scaling to similar device dimensions and bias conditions)[23], we estimate that the noise levels displayed in Fig. 2a are lower by two to three orders of magnitude. We anticipate that this enhanced performance will prove important for quasi-static or low-frequency force or displacement measurements, for example, in contact-mode scanning probe microscopy.

Our piezoresistively detected nanocantilevers are sufficiently sensitive to detect their own thermomechanical fluctuations at high frequencies, in the regime of the fundamental mechanical mode, both in vacuum and at atmospheric pressure. For $Q \gg 1$, the displacement noise spectral density on resonance is $S_z^{1/2} = \sqrt{4k_B TQ/(2\pi f_0 K)}$, where k_B, T, Q, f_0 and K are Boltzmann's constant, absolute temperature, quality factor, resonance

Table 1 Parameters of the four self-sensing nanocantilever devices of this work.

Cantilever	Dimension (µm × µm × µm)	Frequency	Force constant (N m^{-1})	Q at 0.01 torr (300 K)	Q at 1 atm (300 K)	Displacement sensitivity in vacuo at 300 K (m Hz$^{-1/2}$)	Force sensitivity in vacuo at 300 K (aN Hz$^{-1/2}$)
a	33 × 5 × 0.1	52 kHz	5×10^{-3}	500	15	5×10^{-10}	712
b	10 × 2 × 0.1	1.6 MHz	0.15	950	20	1×10^{-12}	510
c	2.7 × 0.8 × 0.1	8 MHz	1.15	1,000	90	1.6×10^{-13}	616
d	0.6 × 0.4 × 0.1	127 MHz	32.1	900	400	3.9×10^{-14}	850

©2007 Nature Publishing Group

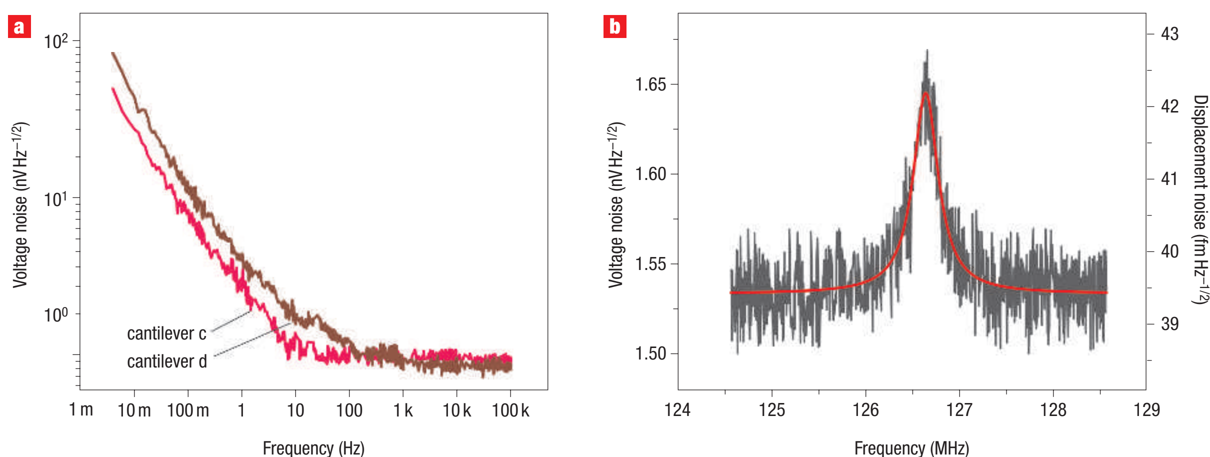

Figure 2 Output voltage noise spectra of high- and very-high-frequency self-sensing nanocantilevers. a, Low-frequency voltage noise spectrum of the 8 and 127 MHz cantilevers (cantilevers c and d). Data are obtained by heterodyne conversion[18] using a 10 mV a.c. bias at 109 Hz. $1/f$ noise knees are measured to be at 8 Hz and 100 Hz, respectively. The larger cantilever 'c' has lower noise than the smaller cantilever 'd', as expected from Hooge's relation. **b**, Noise spectrum from a 127 MHz undriven cantilever (cantilever d), measured at 1 atm and 300 K (black trace). A d.c. bias of 100 mV is used during the measurement. The red line is a Lorentzian fit to thermomechanical noise combined with uncorrelated white background noise. Off-resonance, the displacement sensitivity attained is 39 fm $\mathrm{Hz}^{-1/2}$.

frequency and effective force constant respectively. For the 127 MHz device, the fundamental-mode force constant for end loading is $K \sim 32\ \mathrm{N\,m^{-1}}$, evaluated both analytically and by finite-element simulation. Accordingly, the room temperature displacement noise spectral density expected on resonance is 16 fm $\mathrm{Hz}^{-1/2}$. Figure 2b shows the measured noise spectral density of the 127 MHz cantilever (Fig. 1d) at 300 K and 1 atm. The output voltage noise floor near the 127 MHz resonance, $v_n = (S_T + S_V)^{1/2} \approx 1.53\ \mathrm{nV\,Hz^{-1/2}}$, where S_T is the Johnson noise of the piezoresistive transducer ($R \approx 90\ \Omega$, $S_T^{1/2} = \sqrt{4k_B TR} \approx 1.22\ \mathrm{nV\,Hz^{-1/2}}$) and S_V is the readout amplifier's noise referred to its input, $S_V^{1/2} \approx 0.92\ \mathrm{nV\,Hz^{-1/2}}$ (noise figure ≈ 2 dB at 50 Ω). Thus, at 1 atm, this displacement noise background, referred to the input (displacement domain), corresponds to a resolution of 39 fm $\mathrm{Hz}^{-1/2}$, which is comparable to state-of-the-art optical detection via fibre-optic interferometry[26].

ULTRA-SENSITIVE OPERATION IN AMBIENT

Figure 3 demonstrates a remarkable attribute of nanoscale cantilevers that is displayed here, we believe, for the first time. Compared with their microscale counterparts, the room temperature Q of our smallest devices is only minimally affected in going from high vacuum up to atmospheric pressure. The 127 MHz device exhibits $Q \approx 900$ in vacuum, which decreases only to ∼400 in air at atmospheric pressure. By contrast, the largest device in our family exhibits a factor of 33 decrease over this same range of pressures. Air damping is even more pronounced for larger MEMS-based cantilevers[27]. Figure 3b elucidates the origin of this behaviour. The Q of three cantilevers, having widths of 2 μm, 800 nm and 400 nm, respectively, are plotted versus pressure. These data are fit to a model for gas damping of a cantilever in the molecular flow regime, where

$$Q_m = \left(\frac{\pi}{2}\right)^{3/2} \rho d f_0 \frac{\sqrt{R_0 T/M_0}}{P} \simeq 93 \left(\frac{d}{L}\right)^2 \frac{\sqrt{E\rho}}{P}$$

is predicted for a simple 'diving board' cantilever[28]. Here ρ, d, L and f_0 are the cantilever's density, thickness, length and resonant frequency, respectively, and $R_0 = 8{,}317\ \mathrm{J\,K^{-1}}$ and $M_0 = 29\ \mathrm{kg\,mol^{-1}}$ is the molar mass of air. The observed deviation of the experimental data from this prediction demarcates a crossover from the regime of molecular flow to that of viscous damping[29]. For the three aforementioned devices, this occurs at 30, 300 and 1,000 torr, respectively (Fig. 3, bottom inset). For comparison, the mean free path of air, at 1 atm and room temperature, is about 65 nm.

ATTOGRAM CHEMISORPTIVE MASS SENSING IN AMBIENT

The high Q values we achieve with our nanocantilever devices at atmospheric pressure and room temperature enable ultra-sensitive chemisorptive mass detection in real time, under ambient conditions. The recent milestone of zeptogram-scale (10^{-21} g) nanomechanical mass sensing, by contrast, is carried out at cryogenic temperatures and ultrahigh vacuum (UHV)[12]. In that work, the accretion of gas molecules onto the uncoated, cooled surfaces of the device is enabled simply by physisorption. In the present case we must promote adsorption of a specific target species under ambient conditions—that is, sense a small partial pressure amidst a large background—by engineering chemisorptive accretion. We achieve this by functionalizing the device surface with a thin polymer film having a high partition coefficient for the species of interest[30]. To maintain the nanoresonator's quality factor and frequency, this film must be extremely thin. For our initial demonstration we use polymethyl methacrylate (PMMA)[31], which forms a very thin, conformal layer without the need for elaborate surface treatments. A decrease of only ∼20–30% in the resonance quality factor is typically observed after application of a ∼10 nm coating. Our atmospheric-pressure mass-sensing measurements are carried out on two typical cantilevers operating at resonance frequencies of 8 and 127 MHz (cantilevers c and d), which have calibrated mass responsivities of ∼7 Hz ag^{-1} and ∼0.7 Hz zg^{-1}, respectively.

In separate experiments, these devices are exposed to a series of 1,1-difluoroethane ($C_2H_4F_2$, DFE) gas pulses at room temperature and atmospheric pressure. In response to each, the resonance frequency of the cantilevers first decreases rapidly

©2007 Nature Publishing Group

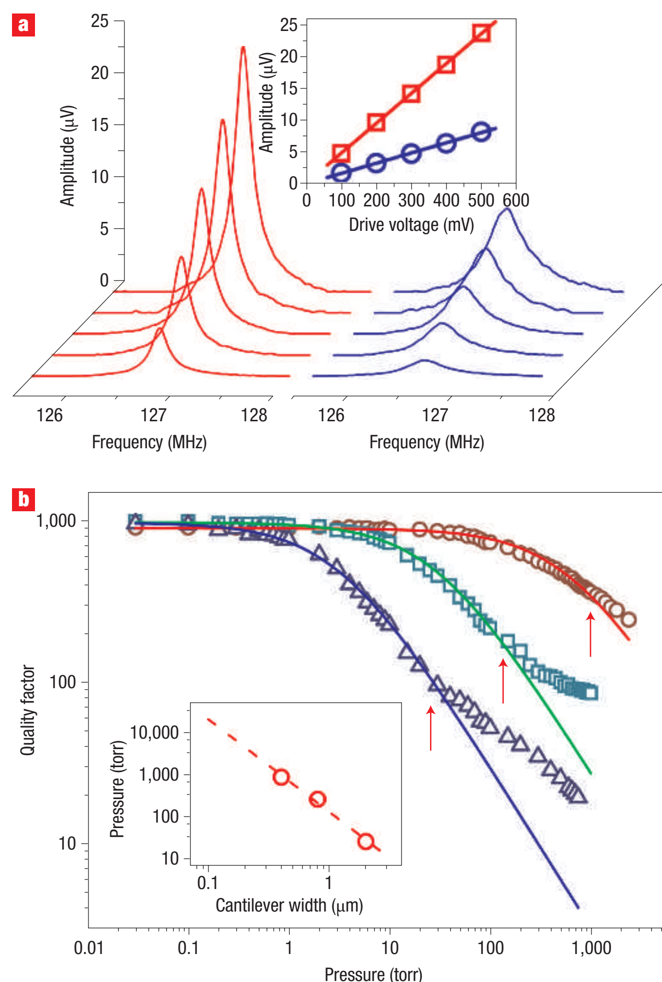

Figure 3 Pressure dependence of the resonance quality factor of a VHF nanocantilever. **a**, Fundamental-mode resonant response of the 127 MHz nanocantilever (cantilever d), in vacuum (red) and at 1 atm (blue), with actuation voltage varying from 100 mV to 500 mV. The inset shows that resonance amplitude is linearly proportional to the actuation drive voltage. **b**, Resonance quality factor for cantilevers b, c and d when operated in air at various pressures. Q factors at 1 atm are 20, 90 and 400, respectively. The measured cantilever Q values (symbols) deviate from predictions based upon molecular flow (solid lines) at the crossover into the viscous flow regime (red arrows). This occurs at 30, 300 and 1,000 torr for the 2-μm, 800-nm and 400-nm wide cantilevers, respectively. The inset shows the relation between the pressure at crossover and cantilever width. Cantilevers b, c and d are shown by triangles, squares and circles respectively.

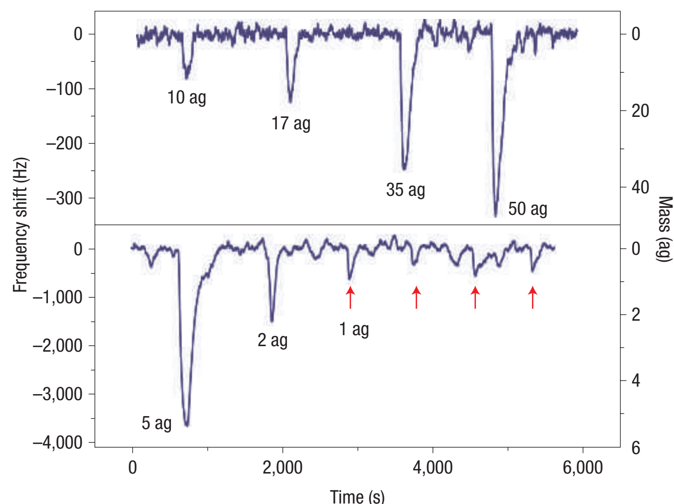

Figure 4 Real-time NEMS chemisorption measurements. 1,1-difluoroethane gas molecules are chemisorbed onto the polymer-coated surfaces of two separate nanocantilever devices. The measurements are carried out in air, at atmospheric pressure and room temperature. The top and bottom traces are measured with 8 MHz and 127 MHz nanocantilevers (cantilevers c and d), respectively. The minimum resolvable mass is below 1 ag (red arrows).

during the injection of gas, then recovers when the injection is completed as the adsorbed gas species slowly desorb from the coating (Fig. 4). This reversible adsorption–desorption process carried out under ambient conditions yields temporal 'dips' of frequency shift, instead of the 'steps' seen in the low-temperature UHV physisorption experiments[12]. Increasing the DFE pulse length yields progressively higher peak mass adsorption of DFE, as is reflected in the increasing mass response dips. As the time constant of the frequency tracking phase-locked loop (PLL) circuitry is set to be 100 ms, the response and recovery time are limited only by the dead volume of the testing chamber. With the 8 MHz cantilever, we are able to resolve mass accretion peaks as small as 10 ag in real time, with mass noise floor ~1 ag. With the 127 MHz cantilever, we achieve the highest mass resolution, estimated to be ~100 zg, allowing mass peaks of 1 ag to be resolved (Fig. 4b).

CONCLUSIONS

To date, AFM has been based solely upon microscale cantilever sensors, despite the fact that the forces detected actually originate from a scanning tip with nanometre dimensions. The straightforward realization of nanometre-scale probes we describe herein can provide optimally matched, low-inertia sensors—that is, nanoscale sensors for nanoscale tips—for transducing such forces. By circumventing the need for optical detection, it now becomes possible to use much smaller cantilevers. This, in turn, enables realization of probes that operate in the previously inaccessible regimes of very high frequency and compliance. High force sensitivity, wide bandwidth and very fast response thereby become possible, crucial attributes for applications such as fast scanning SPM technologies, subpiconewton biological force sensing and VHF force detection (such as required for transverse magnetic resonance force microscopy[32]). We also anticipate that the type of self-sensing nanocantilever probes reported here will prove to be of central importance for a number of other fields. Our self-sensing probes also readily engender scale-up to large-array sensor technologies, simplified 'systems' realizations for portable sensing, and realization of multiple-cantilever sensor elements enabling correlated or stochastic detection[33]. Furthermore, the use of on-chip electronic readout will prove especially advantageous for detection in liquid environments of low or arbitrarily varying optical transparency, as well as for operation at cryogenic temperatures, where maintenance of precise optical component alignment becomes problematic.

An especially compelling attribute of these ultrasmall cantilevers is their unprecedented mass responsivity, $\Re = \partial\omega_0/\partial M_{\rm eff} = -\omega_0/(2M_{\rm eff})$ (ref. 34), where ω_0 and $M_{\rm eff}$ are

©2007 Nature Publishing Group

the resonant frequency and effective mass of the specific mechanical mode used. For uniform reduction of all dimensions of a simple cantilever with linear dimension ℓ, one finds that $\Re \propto 1/\ell^4$. Hence, even making what might at first seem only a minor transition from the micro- to nanoscale can yield a profound sensitivity improvement[9]. For devices with sizes comparable to the mean free path in air, the added benefit of preservation of a high quality factor in ambient enables unprecedented, sub-attogram-scale mass resolution at room temperature and atmospheric pressure, as demonstrated here. These attributes make self-sensing nanometre-scale cantilever resonators a surprisingly versatile and promising platform for chemical, biological and scanned-probe sensing.

METHODS

CANTILEVER NANOFABRICATION

We fabricated nanocantilevers with surface micromachining techniques involving only two processing steps[35]. The starting material is a layer of 70-nm-thick 3C silicon carbide, epitaxially grown on a silicon substrate. The nanocantilever structure is patterned with electron-beam lithography, metal-film deposition and lift-off methods. For the cantilevers shown in the inset of Fig. 1, a 30-nm-thick gold film is used as the transducer layer. This metal overlayer serves as both a mask during the etching process and as a piezoresistive transducer in the completed device. The SiC/metal cantilever is ultimately released from the substrate with chemically selective plasma dry etching.

HIGH-FREQUENCY NEMS CHARACTERIZATION

The cantilever frequency response is measured with a vector network analyser (HP3577A). The sample is mounted on, and actuated by, a piezoceramic actuator. With a d.c./RF bias tee, a d.c. voltage is applied across the device's displacement transducer, and the a.c. signal thus generated piezoresistively by the motion of the device is amplified with a low-noise RF preamplifier. The low impedance of these devices makes direct measurement possible without the loss of bandwidth when frequency modulation methods are used. The resonant response of four devices is displayed in Fig. 1; they are plotted as a resistance change normalized by the d.c. transducer resistance. All of the signals thus acquired use the same biasing and actuation voltage, which are set to deliver a constant 1 nN (10^{-9} N) actuation force.

MEASUREMENT OF LOW-FREQUENCY TRANSDUCER NOISE

A transformer-coupled preamplifier (Stanford Research SR554) was used to match the device resistance to the amplifier's R_{opt}, and thus contribute negligible noise to the measurement. A lock-in amplifier (SR 830) is referenced by an a.c. signal at 109 Hz, which is used to bias the displacement transducer of the device. The demodulated signal from the output of the lock-in amplifier is subsequently fed into a low-frequency FFT spectrum analyser (HP 35665A). With a bias voltage of 10 mV r.m.s. the $1/f$ noise knees are found to be at 8 Hz and 100 Hz for the 8 and 127 MHz devices, respectively.

CALIBRATION OF DISPLACEMENT SENSITIVITY

Cantilever displacement sensitivity for these devices is calibrated by measuring their room-temperature thermomechanical noise spectra. This technique has been proven to be a reliable method and is widely used to calibrate scanning probes in the AFM community. The procedure is illustrated by considering Fig. 2b, where the measured voltage noise spectral density on and off resonance are 1.644 nV $\text{Hz}^{-1/2}$ and 1.519 nV $\text{Hz}^{-1/2}$, respectively. The contribution arising from the cantilever's thermomechanical motion is thus 0.63 nV $\text{Hz}^{-1/2}$, the square root of the difference of their squares. The displacement noise floor on resonance for a 127 MHz cantilever, limited by thermal noise, is $S_z^{1/2} = \sqrt{4k_B TQ/(2\pi f_0 K)} = 16\ \text{fm Hz}^{-1/2}$. Hence we deduce the displacement responsivity (transduction gain) of this self-sensing device as $R_v^z = 0.63\ \text{nV Hz}^{-1/2}/16\ \text{fm Hz}^{-1/2} = 0.04\ \text{nV fm}^{-1}$. We further use this responsivity to evaluate the displacement resolution, imposed by the off-resonance output voltage noise floor referred to the displacement domain using this responsivity, $x_n = \sqrt{S_z} \sim \sqrt{S_{V_{out}}(\omega \neq \omega_0)/R_T^2}$ which yields $x_n \sim (1.519\ \text{nV Hz}^{-1/2})/(0.04\ \text{nV fm}^{-1}) = 39\ \text{fm Hz}^{-1/2}$.

NEMS CHEMISORPTION MEASUREMENTS

To functionalize the sensors, the two smallest devices are spin coated at 4,000 r.p.m. with a solution of 0.5 wt% 495 K PMMA in anisole. The resulting polymer film thickness is approximately 10 nm, as confirmed with both AFM and careful measurement of the change in resonance frequency arising from mass loading by the coating after its application. The mass responsivities[34] of the two devices used in these experiments, $\Re = \partial f/\partial M \sim f_0/2M_{eff}$, are calibrated by separate low-temperature physisorption experiments using a controlled flux of xenon atoms. This procedure is described in more detail elsewhere (ref. 12; Myers, E.B. *et al.* manuscript in preparation). We obtain values of 7 Hz ag^{-1} and 0.68 Hz zg^{-1}, respectively, in good agreement with our predictions from finite-element analysis. These devices are read out using a computer-controlled PLL, which allows us to excite and track the nanocantilevers' resonance frequency in real time[12]. Our setup enables tracking of the resonance frequency of cantilevers in air with a precision better than 10^{-6} (1 ppm) using a time constant of 100 ms. A background of slow frequency drift, which arises from uncompensated thermal drift during the experiments is subtracted. Theoretically, mass resolution is given by the expression[34] $\delta M \sim (M_{eff}/Q) \cdot 10^{-DR/20}$. The 127 MHz cantilever has effective mass $M_{eff} = 100$ fg, dynamic range DR = 80 dB and quality factor $Q \approx 400$ in air. Using these values, we expect a mass resolution of $\sim$25 zg at room temperature. Environmental fluctuations, which include those of temperature, pressure, humidity and so on, apparently degrade our resolution from the observed value of $\sim$100 zg, which is only a factor of four away from ideal performance.

Received 27 September 2006; accepted 1 December 2006; published 28 January 2007.

References

1. Binnig, G., Quate, C. F. & Gerber, C. Atomic force microscope. *Phys. Rev. Lett.* **56,** 930–933 (1986).
2. Binnig, G. *et al.* Atomic resolution with atomic force microscope. *Europhys. Lett.* **3,** 1281–1286 (1987).
3. Meyer, E., Hug, H. J. & Bennewitz, R. *Scanning Probe Microscopy: The Lab on a Tip* (Springer, Berlin, New York, 2004).
4. Wiesendanger, R. *Scanning Probe Microscopy and Spectroscopy: Methods and Applications* (Cambridge Univ. Press, Cambridge, UK, 1994).
5. Lang, H. P. *et al.* Nanomechanics from atomic resolution to molecular recognition based on atomic force microscopy technology. *Nanotechnology* **13,** R29–R36 (2002).
6. Lavrik, N. V., Sepaniak, M. J. & Datskos, P. G. Cantilever transducers as a platform for chemical and biological sensors. *Rev. Sci. Instrum.* **75,** 2229–2253 (2004).
7. Yan, X. D., Ji, H. F. & Thundat, T. Microcantilever (mcl) biosensing. *Curr. Anal. Chem.* **2,** 297–307 (2006).
8. Albrecht, T. R. *et al.* Microfabrication of cantilever styli for the atomic force microscope. *J. Vac. Sci. Technol. A* **8,** 3386–3396 (1990).
9. Roukes, M. Nanoelectromechanical systems face the future. *Phys. World* **14,** 25–31 (February 2001).
10. Cleland, A. N. & Roukes, M. L. A nanometre-scale mechanical electrometer. *Nature* **392,** 160–162 (1998).
11. Rugar, D. *et al.* Single spin detection by magnetic resonance force microscopy. *Nature* **430,** 329–332 (2004).
12. Yang, Y. T. *et al.* Zeptogram-scale nanomechanical mass sensing. *Nano Lett.* **6,** 583–586 (2006).
13. Mamin, H. J. & Rugar, D. Sub-attonewton force detection at millikelvin temperatures. *Appl. Phys. Lett.* **79,** 3358–3360 (2001).
14. Naik, A. *et al.* Cooling a nanomechanical resonator with quantum back-action. *Nature* **443,** 193–196 (2006).
15. Schwab, K. C. & Roukes, M. L. Putting mechanics into quantum mechanics. *Phys. Today* **58,** 36–42 (July 2005).
16. Tortonese, M., Barrett, R. C. & Quate, C. F. Atomic resolution with an atomic force microscope using piezoresistive detection. *Appl. Phys. Lett.* **62,** 834–836 (1993).
17. Parker, R. L. & Krinsky, A. Electrical resistance–strain characteristics of thin evaporated metal films. *J. Appl. Phys.* **34,** 2700–2708 (1963).
18. Jen, S. U. *et al.* Piezoresistance and electrical resistivity of pd, au, and cu films. *Thin Solid Films* **434,** 316–322 (2003).
19. Smith, C. S. Piezoresistance effect in germanium and silicon. *Phys. Rev.* **94,** 42–49 (1954).
20. Kuczynski, G. C. Effect of elastic strain on the electrical resistance of metals. *Phys. Rev.* **94,** 61–64 (1954).
21. Hooge, F. N. 1/f noise is no surface effect. *Phys. Lett. A* **A 29,** 139–140 (1969).
22. Arlett, J. L. *et al.* Self-sensing micro- and nanocantilevers with attonewton-scale force resolution. *Nano Lett.* **6,** 1000–1006 (2006).
23. Harley, J. A. & Kenny, T. W. High-sensitivity piezoresistive cantilevers under 1000 angstrom thick. *Appl. Phys. Lett.* **75,** 289–291 (1999).
24. Femlab 3.1 (Comsol AB, Burlington, MA, USA).
25. Scofield, J. H. AC method for measuring low-frequency resistance fluctuation spectra. *Rev. Sci. Instrum.* **58,** 985–993 (1987).
26. Rugar, D., Mamin, H. J. & Guethner, P. Improved fiber-optic interferometer for atomic force microscopy. *Appl. Phys. Lett.* **55,** 2588–2590 (1989).
27. Yasumura, K. Y. *et al.* Quality factors in micron- and submicron-thick cantilevers. *J. Microelectromech. Syst.* **9,** 117–125 (2000).
28. Newell, W. E. Miniaturization of tuning forks. *Science* **161,** 1320–1326 (1968).
29. Bhiladvala, R. B. & Wang, Z. J. Effect of fluids on the q factor and resonance frequency of oscillating micrometer and nanometer scale beams. *Phys. Rev. E* **69,** 036307 (2004).
30. Grate, J. W. & Abraham, M. H. Solubility interactions and the design of chemically selective sorbent coatings for chemical sensors and arrays. *Sens. Actuator B-Chem.* **3,** 85–111 (1991).

©2007 Nature Publishing Group

31. Battiston, F. M. *et al*. A chemical sensor based on a microfabricated cantilever array with simultaneous resonance-frequency and bending readout. *Sens. Actuator B-Chem.* **77,** 122–131 (2001).
32. Sidles, J. A. *et al*. Magnetic-resonance force microscopy. *Rev. Mod. Phys.* **67,** 249–265 (1995).
33. Arlett, J. L. *et al*. in *Controlled Nanoscale Motion in Biological and Artificial Systems.* Nobel symposium 131, June 2005; ed. Linke, H. *et al.* (Springer-Verlag, Heidelberg, in press).
34. Ekinci, K. L., Yang, Y. T. & Roukes, M. L. Ultimate limits to inertial mass sensing based upon nanoelectromechanical systems. *J. Appl. Phys.* **95,** 2682–2689 (2004).
35. Yang, Y. T. *et al*. Monocrystalline silicon carbide nanoelectromechanical systems. *Appl. Phys. Lett.* **78,** 162–164 (2001).

Acknowledgement

We acknowledge support for this work from DARPA/MTO-MGA through grant NBCH1050001.
Correspondence and requests for materials should be addressed to M.L.R.

Competing financial interests

The authors declare that they have no competing financial interests.

Reprints and permission information is available online at http://npg.nature.com/reprintsandpermissions/

©2007 Nature Publishing Group